

# Understanding the Ion Transport Behavior across Nanofluidic Membranes in Response to the Charge Variations

Linxiao Hou, Weipeng Xian, Shaosuo Bing, Yanpei Song, Qi Sun,\* Lin Zhang, and Shengqian Ma\*

Biological pores regulate the cellular traffic of a diverse collection of molecules, often with extremely high selectivity. Given the ubiquity of charge-based separation in nature, understanding the link between the charged functionalities and the ion transport activities is essential for designing delicate separations, with the correlation being comparatively underdeveloped. Herein, the effect of charge density from the impact of pore structure is decoupled using a multivariate strategy for the construction of covalent organic framework-based membranes. How the density of charged sites in the nanofluidic membranes affect the ion transport activity with particular emphasis on  $\text{Li}^+$  and  $\text{Mg}^{2+}$  ions, relevant to the challenge of salt-lake lithium mining is systematically investigated. Systematic control of the charge distribution produces membranes with numerous advantages, overcoming the long-term challenge of  $\text{Li}^+/\text{Mg}^{2+}$  separation. The top membrane exhibits an outstanding equilibrium selectivity for  $\text{Li}^+$  over  $\text{Mg}^{2+}$  and operational stability under diffusion dialysis and electrodialysis conditions ( $\text{Li}^+/\text{Mg}^{2+}$  up to 500), qualifying it as a potential candidate for lithium extraction. It is anticipated that the developed nanofluidic membrane platform can be further leveraged to tackle other challenges in controlled separation processes.

## 1. Introduction

Nature has adapted over millennia to control complex processes intelligently, with paradigmatic examples of ion transport across the cellular membranes wherein the filter regions are enriched with charged residues.<sup>[1]</sup> To mimic the functions of the biological processes, solid-state nanofluidic membranes were proposed to control the transport of ionic species flowing through them.<sup>[2]</sup> One of the fundamental factors that determine the ion transport activity is the nanoscale control of the surface chemistry of channels.<sup>[3]</sup> For example, it has long been recognized

that ionic species transport profiles can be manipulated through active regulating of surface charge density.<sup>[4]</sup> To fully use such characteristics for more delicate separation processes, a greater understanding of the ion transport behavior, along with the varying charge distribution in the nanofluidic membranes, is essential. However, due to the lack of systematic exploration, such a correlation has yet to be established.


Recent advances in material science render opportunities to address this goal, and a prime example is the advent of two-dimensional covalent organic frameworks (2D COFs).<sup>[5]</sup> The programmability of this type of material offers several essential features that are expected to improve the creation of more sophisticated, controllable separation systems relative to other currently used materials, such as: 1) uniform yet adjustable cylindrical nanochannels in the range of 0.8–4.8 nm, could, in principle, serve as a promising

nanofluidic system; 2) rigid construction could allow the precise organization of functional groups evenly spaced along a 1D channel; and 3) customized synthesis would allow access to an infinite number of charge states in one material, thus enabling control over the transport behavior of analytes. With these attributes, COFs are expected to serve as an ideal platform for creating biomimetic nanofluidic systems with controllable ion transport activity in applications ranging from energy resource recovery to water purification.<sup>[6]</sup>

To investigate the effect of the charge distribution of nanofluidic membranes on the ion transport behavior, we used a multivariate (MTV) strategy, using which the population of a specific functionality could be readily manipulated in one COF without altering the underlying topology,<sup>[7]</sup> thus allowing comparative studies with high fidelity. To regulate the charge population in the membrane, two organic linkers with or without charge were incorporated into one COF structure at various ratios of these two monomers to produce nanochannels with various charge densities.  $\text{Li}^+/\text{Mg}^{2+}$  separation is a critical step in the extraction of lithium from salt-lake brines. Therefore, to meet the increasing demand for this energy-critical element,<sup>[8]</sup> we investigated the influence of the surface charge density of COF channels on the transport profiles of  $\text{Li}^+$  and  $\text{Mg}^{2+}$ , and, consequently, the accompanying separation factor (Figure 1). It was shown that the ion transport process has an even higher degree of complexity. This was inconsistent with the general

Dr. L. Hou, W. Xian, S. Bing, Dr. Q. Sun, Prof. L. Zhang  
College of Chemical and Biological Engineering  
Zhejiang University  
Hangzhou 310027, China  
E-mail: sunqichs@zju.edu.cn

Y. Song, Prof. S. Ma  
Department of Chemistry  
University of North Texas  
1508 W Mulberry St, Denton, TX 76201, USA  
E-mail: shengqian.ma@unt.edu

 The ORCID identification number(s) for the author(s) of this article can be found under <https://doi.org/10.1002/adfm.202009970>.

DOI: 10.1002/adfm.202009970

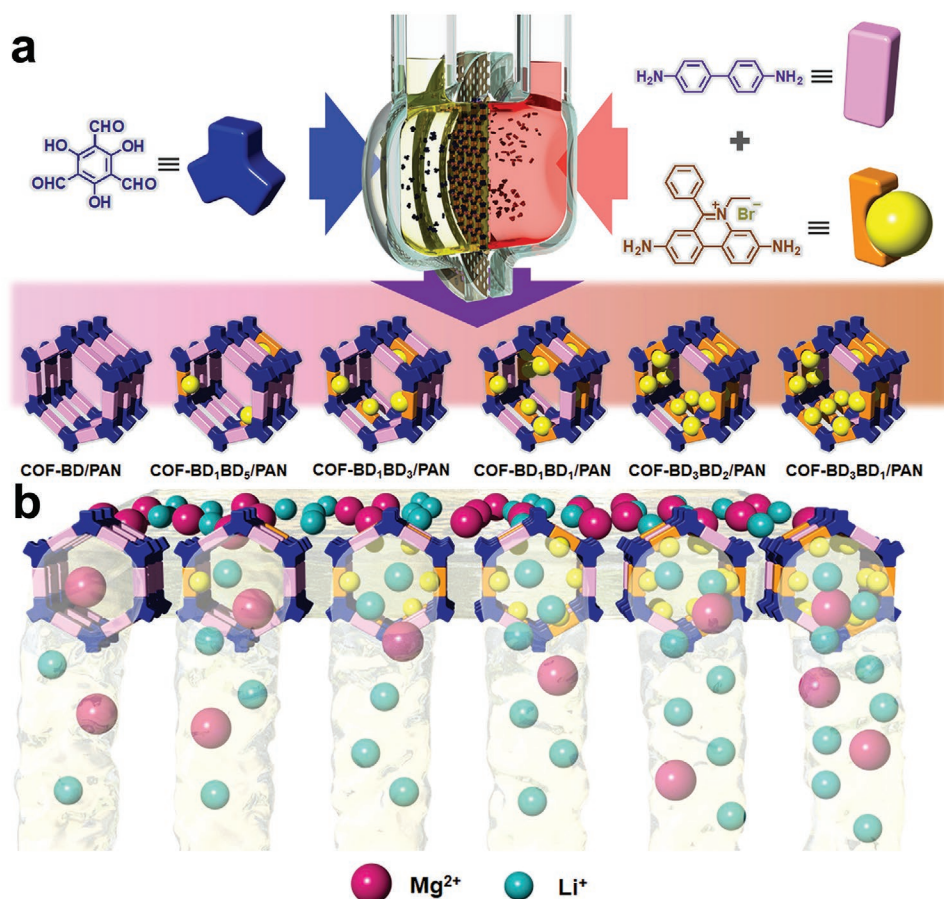


**Figure 1.** a) Synthetic scheme illustration of COF-based membranes with varied charge densities via interface polymerization, and b) diagram illustration of active regulating of surface charge density to manipulate transport profile of Li<sup>+</sup> and Mg<sup>2+</sup> ions.

thinking that when a charged surface is in contact with an electrolyte solution, co-ions are strongly electrostatically repelled when the channel size is comparable to the Debye screening length. In addition, according to the dielectric exclusion principle, the capability of the system to distinguish between monovalent ions and multivalent ions improved with an increase in surface charge density. However, our experimental results show that the charged groups do not always inhibit co-ions from entering the pore channels, but play a pivotal role in facilitating the translocation of Li<sup>+</sup> ions. The permeability of divalent Mg<sup>2+</sup> ions is less related to the charge density of the materials, fluctuating within a small amplitude when this value falls within the range of 0.39–0.78 mmol g<sup>-1</sup>. However, by further increasing the number of charged sites, the permeability of Mg<sup>2+</sup> greatly increases. The established structure-performance relationship can be applied to other separation processes and added to our understanding of ion transport across cellular membranes.

## 2. Results and Discussion

We used the well-known COF constructed by triformylphloroglucinol (Tp) and biphenyl diamine linkers to synthesize MTV-COFs with varying charge densities.<sup>[6b]</sup> To increase the processability, the COF active layers were grown on partially

hydrolyzed polyacrylonitrile (PAN) ultrafiltration membranes (Figure S1, Supporting Information). The use of PAN as the support is mainly based on the following considerations: 1) PAN is flexible, which can increase the operability of the resulting membrane; 2) PAN is hydrophilic and negatively charged, which can lower the transmembrane energy of cations. Interface polymerization was adopted (Figure S2, Supporting Information) to achieve membranes wherein the aqueous solution contained the amine monomers (ethylenediamine (EB) and benzidine (BD)) and a catalyst of *p*-toluenesulfonic acid (TsOH), and the dichloromethane phase contained Tp. The resulting membranes are denoted as COF-EB<sub>x</sub>BD<sub>y</sub>/PAN (*x* and *y* refer to the mole ratio of EB and BD in the membranes synthesis, Figure 1). The color of the resulting membranes ranged from dark yellow to brick red as the proportion of EB increased (Figure S3, Supporting Information). Scanning electron microscopy (SEM) images revealed crack-free, continuous film surfaces that contoured the underlying PAN support with a thickness around 200 nm (Figures S4 and S5, Supporting Information). The surface morphology of the resulting membranes was coarser with the increase of EB (Figure S6, Supporting Information). The elemental mapping distribution collected by an electron microprobe analyzer showed that Br species were homogeneously dispersed throughout the membranes (Figure S7, Supporting Information). Dye molecules

exclusion experiments indicated that the diffusion channel size of the resulting membranes is smaller than the size of methyl blue (2.3 nm, see details in the Experimental Section in the Supporting Information). The  $\beta$ -ketoenamine structures of the resulting COF membranes were confirmed by Fourier transform-infrared spectroscopy (FT-IR) analysis, which showed a new peak at 1593  $\text{cm}^{-1}$  for  $\text{C}=\text{C}$  along with the undetached  $\text{C}=\text{N}$  stretch at around 1620  $\text{cm}^{-1}$ . The disappearance of the stretching signals of the primary amine ( $\nu_{\text{N-H}} \approx 3200 \text{ cm}^{-1}$ ) and aldehyde ( $\nu_{\text{C=O}} = 1642 \text{ cm}^{-1}$ ) indicated the high polymerization degree of the membranes (Figure S8, Supporting Information).<sup>[6b]</sup> The relative intensity of  $\text{C}-\text{N}$  originated from quaternary ammonium displayed a trend of increase along with the proportion of EB increased from 0% to 75% in the synthesis of  $\text{COF-EB}_x\text{BD}_{1-x}/\text{PAN}$  (Figure S8, Supporting Information). The N 1s X-ray photoelectron spectroscopy (XPS) spectra recorded from free-standing  $\text{COF-EB}_x\text{BD}_{1-x}$  ( $x < 1$ ), exhibited two peaks located at 399.6 and 401.3 eV, which are characteristic N 1s signals for the amino N atoms ( $\text{N}-\text{H}$ ), and quaternary ammonium N atoms, respectively, suggestive of the successful incorporation of EB species (Figure S9, Supporting Information).<sup>[9]</sup> The relative intensity of N 1s originating from quaternary ammonium displayed an increasing trend as the proportion of EB increased from 0% to 75% in the synthesis of  $\text{COF-EB}_x\text{BD}_{1-x}/\text{PAN}$ . To quantify the amount of charge sites in the membranes, we evaluated the content of Br species in the membranes by ion chromatography. A positive correlation between the stoichiometry of the starting materials and the actual linker ratios in the resultant COF membranes was observed (Table S1, Supporting Information), validating the XPS and FT-IR results. Powder X-ray diffraction (PXRD) analysis of the free-standing  $\text{COF-EB}_x\text{BD}_{1-x}$  membranes revealed crystalline structures with a prominent peak at  $3.7^\circ$  and a relatively broad peak at  $27.1^\circ$ , assigned to the (100) and (001) facets, respectively. The PXRD patterns for the samples were qualitatively identical to each other, verifying that they were isostructural (Figure S10, Supporting Information). The diffraction patterns matched well with the calculated pattern based on the eclipsed stacking structures.  $\text{N}_2$  sorption isotherms collected at 77 K revealed that the accessible size of the free-standing  $\text{COF-EB}_1\text{BD}_1$  membrane is around 2 nm, in line with the eclipsed stacking model (Figure S11, Supporting Information). The zeta potentials of the  $\text{COF-EB}_x\text{BD}_{1-x}/\text{PAN}$  membranes were less negative than those of pristine PAN, varying within a small range from  $-25.8$  to  $-15.6$  mV for the samples containing EB, which suggested the positive charge of the COF layers and the homogeneous distribution of charged moieties throughout the pore channels (Figure S12, Supporting Information). This assumption was further supported by their greatly increased zeta potentials in the powder form and similar surface wettability (Table S2 and Figure S13, Supporting Information).

Lithium batteries have changed the world and are ubiquitous in modern society, and power most of the electronics that we use. To meet the continuously growing demand for lithium, the development of technology capable of economically extracting lithium from low-grade deposits would ensure resource accessibility, which ultimately promotes investment in this mature energy storage technology.<sup>[8]</sup> The effective discrimination between  $\text{Li}^+$  and  $\text{Mg}^{2+}$  ions is especially problematic in lithium

extraction from brine because of their similar properties in terms of reactivity. Given the restriction of Donnan exclusion and electroneutrality requirements, there are different influences of charged channels on the transport profiles of ions with different valences, which can consequently offer ion selectivity.<sup>[10]</sup> These considerations prompted us to pursue the separation of lithium and magnesium using these membranes. We tested the initial diffusion fluxes of  $\text{Li}^+$  and  $\text{Mg}^{2+}$  across these membranes to quantitatively compare their transmembrane activity. A home-made U-shaped dual-chamber diffusion cell was used. Single ion diffusion profiles were collected with a  $\text{LiCl}$  or  $\text{MgCl}_2$  concentration of 0.1 M. The amount of ions transported from the feed chamber to the permeate chamber were recorded using a conductivity meter. The transport kinetics were reflected in the slope of ion concentration in the permeate chamber versus operation time. The ion diffusion flux and  $\text{Li}^+/\text{Mg}^{2+}$  separation factor were calculated from the slope of the permeation curves. All tested membranes showed higher permeability of  $\text{Li}^+$  ions than  $\text{Mg}^{2+}$  ions. We also ran control tests of the membrane in the absence of EB, which showed negligible ion transport activity, highlighting the role of charged sites as ion transporters (Figure 2a). Correlating the initial  $\text{Li}^+$  and  $\text{Mg}^{2+}$  transport rates to the synthesized membranes showed that the charge density was a determinant of ion transport. The transport rate of  $\text{Mg}^{2+}$  and  $\text{Li}^+$  ions differed considerably in response to the varied charge densities of the membranes. The permeability of  $\text{Li}^+$  ions increases with an increase in the charge population, as reflected by the gradually steeper slopes, whereas the transport of  $\text{Mg}^{2+}$  ions across the membranes was more complicated, displaying a trend of increasing, decreasing, and then increasing.  $\text{COF-EB}_3\text{BD}_1/\text{PAN}$ , with the highest charge density among the membranes tested, did not exhibit the best  $\text{Li}^+/\text{Mg}^{2+}$  selectivity, and this value was not even close to the highest (Figure 2a). This was counterintuitive because usually, the higher the charge site concentration, the more effective the membrane is in rejecting high-valent co-ions and, consequently, the higher the  $\text{Li}^+/\text{Mg}^{2+}$  separation factor. In comparison,  $\text{COF-EB}_1\text{BD}_1/\text{PAN}$ , with a much lower charge density, exhibited the highest  $\text{Li}^+/\text{Mg}^{2+}$  separation factor. Considering that the COFs were isostructural, and the resulting membranes show a similar thickness, the impact of the dynamic resistance of the membrane can be excluded. Therefore, we rationalized these trends using Donnan membrane equilibrium. As electrostatic forces from the charged sites on membranes cause counter-ions to move in the direction of their concentration gradient; this leads to the enrichment of nanochannels with counter-ions and depleted co-ions.<sup>[11]</sup> In combination with the requirement of electroneutrality, there is a competition between electrostatic repulsion of co-ions against the charged nanochannels and the electrostatic attraction from counter-ions filled in the nanochannels. Given a balanced electrostatic interaction with monovalent co-ions and counter-ions, the transport rate of  $\text{Li}^+$  ions accelerates as the charge density increases as more  $\text{Cl}^-$  ions are enriched. This is in stark contrast to the transport of  $\text{Mg}^{2+}$  ions, which exhibited an increase, decrease, and another increase in response to the increased charge density. We postulated that the electrostatic repulsion that dominates the permeation of  $\text{Mg}^{2+}$  ions with the membrane charge density falls in the range of  $0\text{--}0.59 \text{ mmol g}^{-1}$  ( $x/y$  in  $\text{COF-EB}_x\text{BD}_y/\text{PAN}$  is

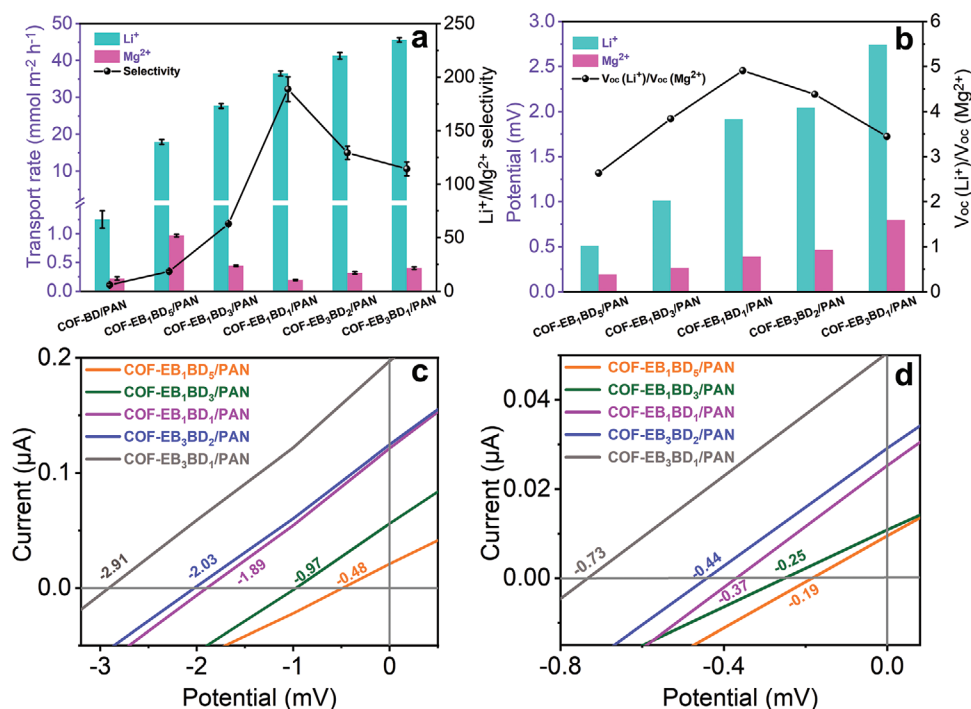


**Figure 2.** a) The transport rate of Li<sup>+</sup> and Mg<sup>2+</sup> across various membranes and the corresponding Li<sup>+</sup>/Mg<sup>2+</sup> selectivity under diffusion dialysis with a LiCl or MgCl<sub>2</sub> concentration of 0.1 M, respectively. b,c) *I*-*V* curves of the synthesized membranes measured in 0.1 M salt solutions based on the concentration of Cl<sup>-</sup> ions. d) The summary of V<sub>oc</sub> values and their corresponding ratios obtained from (b and c).

less than 1). This is because of the dielectric exclusion controls; the exclusion from a charged layer is more rigorous for a bivalent co-ion compared to a monovalent ion. However, as the charge density increases further, the attraction of enriched counter-ions dominates over the repulsion of high-valent cations, thereby accelerating the transmembrane permeation of Mg<sup>2+</sup> ions. These factors cause the Li<sup>+</sup>/Mg<sup>2+</sup> separation factor to increase first and then decrease. COF-EB<sub>1</sub>BD<sub>1</sub>/PAN appears to be the best material among this series.

To quantitatively evaluate the preferred transport of Li<sup>+</sup> over Mg<sup>2+</sup> ions, their relative transmembrane permeability was evaluated. Given that the potential of zero current (V<sub>oc</sub>) is related to the permeability of ions in the contact solutions located at the two sides of the membrane, current-voltage (*I*-*V*)

curves were collected. To obtain the relative permeability of cations, salt solutions with the same gradient of anions were employed. Upon evaluating the V<sub>oc</sub> in response to the EB proportion in the membrane, a remarkably sharp volcano-type effect was observed (Figure 2b-d). COF-EB<sub>1</sub>BD<sub>1</sub>/PAN exhibited the highest selectivity for lithium over magnesium, according to the Goldman-Hodgkin-Katz equation, which is consistent with the aforementioned results.<sup>[12]</sup>

To further explore the relationship between the membrane charge density and apparent mass transport for Li<sup>+</sup> and Mg<sup>2+</sup> ions that traverse the membranes under various feed concentration conditions, the ion transport profiles of each COF membrane were plotted against the operation time (Figures S14-S19, Supporting Information). All data points converged to reveal a

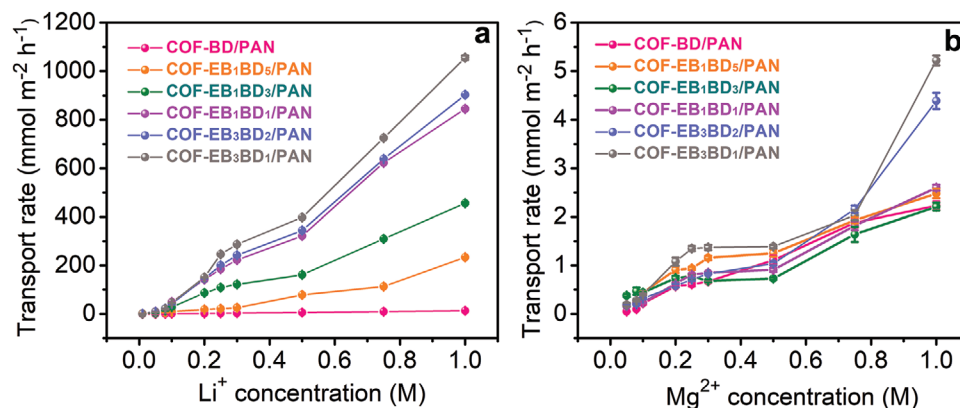


**Figure 3.** The transport rates of Li<sup>+</sup> and Mg<sup>2+</sup> a) and b) across membranes with different charge density under diffusion dialysis with various LiCl or MgCl<sub>2</sub> concentrations ranged from 0.05 to 1 M.

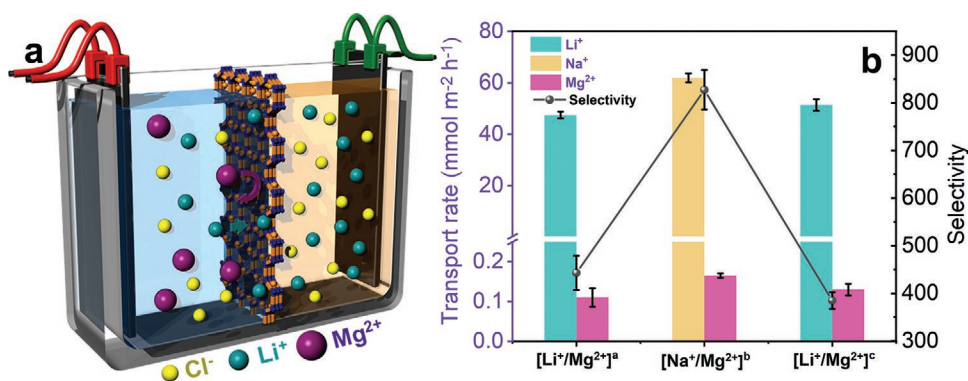


**Figure 4.** a) The schematic diagram illustrating the configuration of the set-up of electrodesalination for ionic permeation measurement. b) Binary Li<sup>+</sup>/Mg<sup>2+</sup> and Na<sup>+</sup>/Mg<sup>2+</sup> selectivities of COF-EB<sub>1</sub>BD<sub>1</sub>/PAN over various conditions. <sup>a</sup>)The 1:1 binary solution (0.1 m each) of LiCl and MgCl<sub>2</sub>; <sup>b</sup>)The 1:1 binary solution (0.1 m each) of NaCl and MgCl<sub>2</sub>; <sup>c</sup>)Artificial brine with the mass ratio of magnesium (29.9 g L<sup>-1</sup>) and lithium (0.85 g L<sup>-1</sup>) of about 35.

linear relationship. **Figure 3** depicts the feed solution concentration-profiled diffusion flux values. The transport patterns of Li<sup>+</sup> and Mg<sup>2+</sup> depending on the change in the ionic strength of the solution were similar to those of the membranes with different charge populations. Except for the neutral membrane, the ion transport rate was not proportional to the feed concentration, suggesting a crucial role of electrostatic interactions in ion transport. The Li<sup>+</sup> ion diffusion rates for the COF-EB<sub>x</sub>BD<sub>1-x</sub>/PAN membranes were nearly linearly increased when the concentration of feed solution increased from 0.05 to 1.0 m. Conversely, the Mg<sup>2+</sup> transport profile slightly increased when the salt concentration increased from 0.05 to 0.2 m, displayed a trend of smoothing when the salt concentration was in a range from 0.2 to 0.5 m, and then greatly increased when the salt concentration further increased from 0.5 to 1.0 m. Therefore, there is a dramatic rise in the Li<sup>+</sup>/Mg<sup>2+</sup> separation factor from 60 to 353 upon increasing the salt concentration from 0.05 to 0.5 m, which reveals that variations in the ion concentration produce significant changes in the membrane selectivity (Figure S20, Supporting Information).

We also tested the transmembrane activities of other cations. Given the superior performance of COF-EB<sub>1</sub>BD<sub>1</sub>/PAN, it was chosen for further studies, which revealed the preferred monovalent cation transport over that of divalent cations. Specifically, the separation factors for H<sup>+</sup>/Mg<sup>2+</sup>, Na<sup>+</sup>/Mg<sup>2+</sup>, Li<sup>+</sup>/Mg<sup>2+</sup>, and Ca<sup>2+</sup>/Mg<sup>2+</sup> were 3094, 360, 353, and 0.62, respectively, under electrolyte concentrations of 0.5 m (Figure S21, Supporting Information). These results can be rationalized by the mobility for the cation ions, following the trend of H<sup>+</sup> > Na<sup>+</sup> > Li<sup>+</sup> > Mg<sup>2+</sup> > Ca<sup>2+</sup>.<sup>[13]</sup>

These results are a promising proof-of-principle that shows that these membranes can be used for Li<sup>+</sup> extraction from salt lakes. According to the established correlations between the salt concentration and Li<sup>+</sup>/Mg<sup>2+</sup> separation factor, an equimolar binary mixture of LiCl and MgCl<sub>2</sub> (0.5 m each) was applied to test the separation performance of COF-EB<sub>1</sub>BD<sub>1</sub>/PAN. To obtain critical mechanistic insight, we tracked the kinetics of ion permeation through these membranes as a function of time (Figure S22, Supporting Information). As expected, the concentrations of Li<sup>+</sup> and Mg<sup>2+</sup> in the permeate increased linearly with time. The comparison of flux and selectivity between single and binary salt mixture measurements

over the COF-EB<sub>1</sub>BD<sub>1</sub>/PAN membranes showed that the fluxes of both Li<sup>+</sup> and Mg<sup>2+</sup> ions decreased under binary salt conditions. The greater decline of Mg<sup>2+</sup> flux relative to Li<sup>+</sup> ions resulted in higher binary Li<sup>+</sup>/Mg<sup>2+</sup> selectivity, compared to the ideal selectivity (505 and 353), placing it among the top materials (Table S3, Supporting Information). We ascribed the decreased flux to the concentration polarization. This is probably due to the negative zeta potential of the membranes causing local accumulation of cations, resulting in lower solute permeance.<sup>[14]</sup> Further research is required to attenuate the concentration polarization and to understand the impact of the support charge on the performance of the active layer. However, the more significant Li<sup>+</sup>/Mg<sup>2+</sup> selectivity can most likely be attributed to the competition mechanism in which Li<sup>+</sup> ions can more easily penetrate the positively charged pore channel than Mg<sup>2+</sup>, and once Li<sup>+</sup> ions are present in the channel, Mg<sup>2+</sup> ions are excluded.

The outstanding separation performance under high ionic strength conditions makes COF-EB<sub>1</sub>BD<sub>1</sub>/PAN promising for extracting lithium from salt lakes. To evaluate the lithium and magnesium separation performance in the real system, an artificial brine with a mass ratio of magnesium (29.9 g L<sup>-1</sup>) and lithium (0.85 g L<sup>-1</sup>) of ≈35 was prepared. This ratio was ≈28.1/1 (mole ratio of Li<sup>+</sup>/Mg<sup>2+</sup>) in the second permeate chamber after a single pass through COF-EB<sub>1</sub>BD<sub>1</sub>/PAN, approaching the battery-grade purity.

To explore the potential of COF-EB<sub>1</sub>BD<sub>1</sub>/PAN in practical operation, electrodesalination was conducted for Li<sup>+</sup>/Mg<sup>2+</sup> separation using a setup relevant to the industry (**Figure 4**; see details in the Experimental Section in the Supporting Information). Excellent selectivity was achieved with Li<sup>+</sup>/Mg<sup>2+</sup> and Na<sup>+</sup>/Mg<sup>2+</sup> separation factors of 443 and 827, respectively, for the 1:1 binary solution (0.1 m each) at a current density of 0.5 mA cm<sup>-2</sup>. Accordingly, the mole ratio of Li<sup>+</sup>/Mg<sup>2+</sup> in the simulated Yiliping brine (Qinghai province in China with magnesium and lithium concentrations of 0.83 mol L<sup>-1</sup> and 0.031 mol L<sup>-1</sup>, respectively) significantly increased from 0.0377 to 385 after electrodesalination. In addition to the separation factor, long-term stability is another essential criterion for practical applications. Negligible loss in permeability and selectivity was observed for COF-EB<sub>1</sub>BD<sub>1</sub>/PAN after continuous operations under electrodesalination conditions for

10 h as well as 2 months under various dialysis conditions. The comprehensive stability under various harsh conditions makes COF-EB<sub>1</sub>BD<sub>1</sub>/PAN a promising candidate for practical lithium extraction.

### 3. Discussion

In summary, we demonstrated that the high intrinsic modularity of COFs allows for precise compositional tuning for the optimization of a membrane's ion-transport activity. This culminated in the discovery of high-performance nanofluidic separation systems, by identifying the critical parameters for improving the separation performance of membranes. In this contribution, we built on the isoreticular principle to show that the ion transport profiles across nanofluidic membranes can be tuned by systematically introducing ionic functionality, as demonstrated by how the charge site distribution could be used to control the transport profile of ions with different valences. This work provides critical mechanistic insights into ion transport at the nanoscale and a rational approach for optimizing membrane performance, with implications for achieving a greater understanding of the functions of ion channels in cell membranes, which ultimately enhances the development of membrane science.

### Supporting Information

Supporting Information is available from the Wiley Online Library or from the author.

### Acknowledgements

L.H. and W.X. contributed equally to this work. The authors acknowledge the National Science Foundation of China (21776241, 2196116074, 222071132), and the Fundamental Research Funds for the Central Universities (17221012001). Partial support from the Robert A. Welch Foundation (B-0027) is also acknowledged (SM).

### Conflict of Interest

The authors declare no conflict of interest.

### Data Availability Statement

The data that support the findings of this study are available on request from the corresponding author. The data are not publicly available due to privacy or ethical restrictions.

### Keywords

biomimetic ionic channels, covalent organic framework membranes, ion separation, lithium extraction, nanofluidic membranes

Received: December 7, 2020

Revised: December 19, 2020

Published online:

- [1] a) Y.-M. Tu, W. Song, T. Ren, Y.-X. Shen, R. Chowdhury, P. Rajapaksha, T. E. Culp, L. Samineni, C. Lang, A. Thokkadam, D. Carson, Y. Dai, A. Mukthar, M. Zhang, A. Parshin, J. N. Sloan, S. H. Medina, M. Grzelakowski, D. Bhattacharya, W. A. Phillip, E. D. Gomez, R. J. Hickey, Y. Wei, M. Kumar, *Nat. Mater.* **2020**, *19*, 347; b) E. Gouaux, R. MacKinnon, *Science* **2005**, *310*, 1461; c) D. A. Doyle, J. M. Cabral, R. A. Pfuetzner, A. Kuo, J. M. Gulbis, S. L. Cohen, B. T. Chait, R. MacKinnon, *Science* **1998**, *280*, 69.
- [2] a) X. Hou, H. Zhang, L. Jiang, *Angew. Chem., Int. Ed.* **2012**, *51*, 2; b) C. R. Martin, Z. S. Siwy, *Science* **2007**, *317*, 331; c) J. Wang, Z. Zhang, J. Zhu, M. Tian, S. Zheng, F. Wang, X. Wang, L. Wang, *Nat. Commun.* **2020**, *11*, 3540.
- [3] a) G. Pérez-Mitta, J. S. Tuninetti, W. Knoll, C. Trautmann, M. E. Toimil-Molare, O. Azzaroni, *J. Am. Chem. Soc.* **2015**, *137*, 6011; b) M. Tagliazucchi, O. Peleg, M. Kröger, Y. Rabin, I. Zleifer, *Proc. Natl. Acad. Sci. U. S. A.* **2013**, *110*, 3363.
- [4] a) X. He, Y. Yang, H. Wu, G. He, Z. Xu, Y. Kong, L. Cao, B. Shi, Z. Zhang, C. Togsh, K. Jiao, K. Zhu, Z. Jiang, *Adv. Mater.* **2020**, *32*, 2001284; b) Y. Guo, Y. Ying, Y. Mao, X. Peng, B. Chen, *Angew. Chem., Int. Ed.* **2016**, *55*, 15120; c) A. E. Childress, M. Elimelech, *Environ. Sci. Technol.* **2000**, *34*, 3710; d) A. Somrani, A. H. Hamzaoui, M. Pontie, *Desalination* **2013**, *317*, 184; e) R. Tan, A. Wang, R. Malpass-Evans, R. Williams, E. W. Zhao, T. Liu, C. Ye, X. Zhou, B. P. Darwich, Z. Fan, Z. Fan, L. Turcani, E. Jackson, L. Chen, S. Y. Chong, T. Li, K. E. Jelfs, A. I. Cooper, N. P. Brandon, C. P. Grey, N. B. McKeown, Q. Song, *Nat. Mater.* **2020**, *19*, 195; f) M. A. Shehzad, Y. Wang, A. Yasmin, X. Ge, Y. He, X. Liang, Y. Zhu, M. Hu, X. Xiao, L. Ge, C. Jiang, Z. Yang, M. D. Guiver, L. Wu, T. Xu, *Angew. Chem., Int. Ed.* **2019**, *58*, 12646; g) M. Zhang, K. Guan, Y. Ji, G. Liu, W. Jin, N. Xu, *Nat. Commun.* **2019**, *10*, 1253; h) X. Li, H. Zhang, H. Yu, J. Xia, Y.-B. Zhu, H.-A. Wu, J. Hou, J. Lu, R. Ou, C. D. Easton, C. Selomulya, M. R. Hill, L. Jiang, *Adv. Mater.* **2020**, *32*, 2001777; i) J. Lu, H. Zhang, J. Hou, X. Li, X. Hu, Y. Hu, C. D. Easton, Q. Li, C. Sun, A. W. Thornton, M. R. Hill, X. Zhang, G. Jiang, J. Z. Liu, A. J. Hill, B. D. Freeman, L. Jiang, H. Wang, *Nat. Mater.* **2020**, *19*, 767; j) Z.-Y. Jiang, H.-L. Liu, S. A. Ahmed, S. Hanif, S.-B. Ren, J.-J. Xu, H.-Y. Chen, X.-H. Xia, K. Wang, *Angew. Chem., Int. Ed.* **2017**, *56*, 4767; k) K. Xiao, L. Chen, Z. Zhang, G. Xie, P. Li, X.-Y. Kong, L. Wen, L. Jiang, *Angew. Chem., Int. Ed.* **2017**, *56*, 8168.
- [5] a) Y. Song, Q. Sun, B. Aguila, S. Ma, *Adv. Sci.* **2019**, *6*, 1801410; b) K. Geng, T. He, R. Liu, S. Dalapati, K. T. Tan, Z. Li, S. Tao, Y. Gong, Q. Jiang, D. Jiang, *Chem. Rev.* **2020**, *120*, 8814; c) X. Guan, F. Chen, Q. Fang, S. Qiu, *Chem. Soc. Rev.* **2020**, *49*, 1357; d) X. Han, C. Yuan, B. Hou, L. Liu, H. Li, Y. Liu, Y. Cui, *Chem. Soc. Rev.* **2020**, *49*, 6248; e) S. Kandambeth, K. Dey, R. Banerjee, *J. Am. Chem. Soc.* **2019**, *141*, 1807; f) M. S. Lohse, T. Bein, *Adv. Funct. Mater.* **2018**, *28*, 1705553; g) Y. Jin, Y. Hu, W. Zhang, *Nat. Rev. Chem.* **2017**, *1*, 0056; h) X. Guan, H. Li, Y. Ma, M. Xue, Q. Fang, Y. Yan, V. Valtchev, S. Qiu, *Nat. Chem.* **2019**, *11*, 228; i) J. W. Colson, A. R. Woll, A. Mukherjee, M. P. Levendorf, E. L. Spitler, V. B. Shields, M. G. Spencer, J. Park, W. R. Dichtel, *Science* **2011**, *332*, 228.
- [6] a) L. Valentino, M. Matsumoto, W. R. Dichtel, B. J. Mariñas, *Environ. Sci. Technol.* **2017**, *51*, 14352; b) H. S. Sasmal, A. Halder, S. Kunjattu H., K. Dey, A. Nadol, T. G. Ajithkumar, P. R. Bedadur, R. Banerjee, *J. Am. Chem. Soc.* **2019**, *141*, 20371; c) C. Yuan, X. Wu, R. Gao, X. Han, Y. Liu, Y. Long, Y. Cui, *J. Am. Chem. Soc.* **2019**, *141*, 20187; d) Q. Hao, Z.-J. Li, C. Lu, B. Sun, Y.-W. Zhong, L.-J. Wan, D. Wang, *J. Am. Chem. Soc.* **2019**, *141*, 19831; e) H. Yang, L. Yang, H. Wang, Z. Xu, Y. Zhao, Y. Luo, N. Nasir, Y. Song, H. Wu, F. Pan, Z. Jiang, *Nat. Commun.* **2019**, *10*, 2101; f) R. Wang, X. Shi, A. Xiao, W. Zhou, Y. Wang, *J. Membr. Sci.* **2018**, *566*, 197; g) D. B. Shinde, G. Sheng, X. Li, M. Ostwal, A.-H. Emwas, K.-W. Huang, Z. Lai, *J. Am. Chem. Soc.* **2018**, *140*, 14342; h) M. Ratsch, C. Ye, Y. Yang, A. Zhang, A. M. Evans, K. Börjesson, *J. Am. Chem. Soc.* **2020**, *142*,

- 6548; i) V. A. Kuehl, J. Yin, P. H. Duong, B. Mastorovich, B. Newell, K. D. Li-Oakey, B. A. Parkinson, J. O. Hoberg, *J. Am. Chem. Soc.* **2018**, *140*, 18200; j) H. Fan, A. Mundstock, A. Feldhoff, A. Knebel, J. Gu, H. Meng, J. Caro, *J. Am. Chem. Soc.* **2018**, *140*, 10094; k) Y. Li, X. Guo, X. Li, M. Zhang, Z. Jia, Y. Deng, Y. Tian, S. Li, L. Ma, *Angew. Chem., Int. Ed.* **2020**, *59*, 4168; l) Y. Ying, M. Tong, S. Ning, K. Ravi, S. B. Peh, S. C. Tan, S. J. Pennycook, D. Zhao, *J. Am. Chem. Soc.* **2020**, *142*, 4472; m) Y. Li, Q. Wu, X. Guo, M. Zhang, B. Chen, G. Wei, X. Li, S. Li, L. Ma, *Nat. Commun.* **2020**, *11*, 599.
- [7] a) Q. Sun, Y. Pan, X. Wang, H. Li, J. Farmakes, B. Aguila, Z. Yang, S. Ma, *Chem* **2019**, *5*, 3184; b) Q. Sun, Y. Tang, B. Aguila, S. Wang, F.-S. Xiao, P. K. Thallapally, A. M. Al-Enizi, A. Nafady, S. Ma, *Angew. Chem., Int. Ed.* **2019**, *58*, 8670.
- [8] a) A. Razmjou, M. Asadnia, E. Hosseini, A. H. Korayem, V. Chen, *Nat. Commun.* **2019**, *10*, 5793; b) S. Yang, F. Zhang, H. Ding, P. He, H. Zhou, *Joule* **2018**, *2*, 1648.
- [9] H. Ma, B. Liu, B. Li, L. Zhang, Y.-G. Li, H.-Q. Tan, H.-Y. Zang, G. Zhu, *J. Am. Chem. Soc.* **2016**, *138*, 5897.
- [10] a) H. Daiguji, *Chem. Soc. Rev.* **2010**, *39*, 901; b) L. Bocquet, E. Charlaix, *Chem. Soc. Rev.* **2010**, *39*, 1073.
- [11] M. Tagliazucchi, I. Szleifer, *Mater. Today* **2015**, *18*, 131.
- [12] W. Sparreboom, A. van den Berg, J. C. T. Eijkel, *Nat. Nanotechnol.* **2009**, *4*, 713.
- [13] L. Cao, W. Guo, W. Ma, L. Wang, F. Xia, S. Wang, Y. Wang, L. Jiang, D. Zhu, *Energy Environ. Sci.* **2011**, *4*, 2259.
- [14] F. Fornasiero, H. G. Park, J. K. Holt, M. Stadermann, C. P. Grigoropoulos, A. Noy, O. Bakajin, *Proc. Natl. Acad. Sci. U. S. A.* **2008**, *105*, 17250.